International Conference on Space Optics—ICSO 2018

Chania, Greece

9–12 October 2018

Edited by Zoran Sodnik, Nikos Karafolas, and Bruno Cugny

Acousto-optic interaction model with mercury halides (Hg2Cl2 and Hg2Br2) as AOTF cristals

A. Pierson

C. Philippe

International Conference on Space Optics — ICSO 2018, edited by Zoran Sodnik, Nikos Karafolas, Bruno Cugny, Proc. of SPIE Vol. 11180, 1118064 · © 2018 ESA and CNES · CCC code: 0277-786X/18/$18 · doi: 10.1117/12.2536139

Acousto-optic interaction model with mercury halides (Hg2Cl2 and Hg2Br2) as AOTF crystals.

A. Pierson[a], C. Philippe*[a]
[a]Altran Technologies, 2 rue Paul Dautier, Vélizy-Villacoublay 78140, France;
*charles.philippe@altran.com

ABSTRACT

Acousto-optic tunable filters (AOTF) are used in the development of hyperspectral imagers from the ultra violet (UV) to the long wave infrared (LWIR). They have the advantage to be an all-solid-state and robust device with no-moving parts that can fast tune their filtered frequency carrier. Such a device is developed by bonding a piezoelectric transducer on a specially cut birefringent crystal. In the LWIR there is a global investigation on efficient solutions for AOTF in future spectral filtering applications. Crystal of mercurous chloride (Hg_2Cl_2) and mercurous bromide (Hg_2Br_2) are candidates that demonstrate an advantage in this spectral domain, thanks to a broadband transparency and a fairly large value of their figure of merit M_2. Industrial development of those crystals has recently started and presents an excellent opportunity to prospect feasibility of such AOTF development. The purpose of our work is to develop a numerical tool to have a better understanding of the acousto-optic interaction inside mercurous halides crystals. Unfortunately, all the characteristics of those mercurous halides based crystals are not well known nowadays. One important component of the photoelastic tensor is always missing. It implies that the unique interaction configuration that optimizes the diffraction efficiency for a wavelength range can't be computed analytically with the usual techniques. To overcome this difficulty, we propose a numerical tool based on an acousto-optic interaction and an acoustic wave propagation models. We will also include the AOTF considerations and the theoretical background needed to carry out the filter design.

Keywords: AOTF, hyperspectral imagers, mercury halides, calomel, Acousto-optic interaction, numerical model

1. INTRODUCTION

An Acousto-optic tunable filter (AOTF) is a device with no-moving parts that can provide an electronically tuned band pass filter by the application of a radiofrequency (RF) signal. The main emphasis is on the development of all solid state compact field-portable imagers from ultraviolet (UV) to long wave infrared (LWIR). Such a device is developed in a birefringent crystal by bonding a piezoelectric transducer to a specially cut prism[1-5]. Acousto-optic (AO) interactions diffract a narrowband part of a white broadband light incident to the input facet of a birefringent crystal that is transparent in the optical wavelength region of interest. This transmitted wavelength band can be tuned by varying the applied RF. Compared to other traditional dispersive optical elements like grating or prism, AOTF devices have slow response time that allows having a high-tuning speed optical bandpass filter.

A spectrometer or hyperspectral imager based on an AOTF in front of a two-dimensional focal plan array (2D-FPA) captures a hyperspectral image cube by scanning the wavelengths in a time sequence to cover the spectral range of operations. This image cube is recorded in a much simpler manner without any relative motion of the scene and the imager compared to a dispersive system such as a grating or a prism. Scenes of interest from hyperspectral activities are in the three atmospheric window regions, visible up to short wave infrared (VIS+NIR+SWIR : from 400 nm to 2.5 µm), medium wave infrared (MWIR : from 3 to 5 µm) and the long wave infrared (LWIR : from 8 to 14 µm). The first two regions are used for enhanced vision for various applications. The latter region is preferred to obtain spatial and spectral signatures from a rich number of chemical, biological species and all objects around 300K.

A number of spectral imagers using AOTF operating from the UV to the LWIR using KDP[6-8], TeO_2[10-15], MgF_2[9] and Tl_3AsSe_3[16-20] crystals to cover different spectral regions have been developed. Commonly, the Tl_3AsSe_3 crystals also named as TAS are used as AO materials for the LWIR region. Nevertheless, there is a lack of high quality AO materials and global research is going on in the test of new materials. We bring our interest on a recently synthesized class of

crystals for having superior properties in AO devices. The mercurous halide crystals[21-26], such as Hg_2Cl_2 (i.e. Calomel), Hg_2Br_2 and Hg_2I_2 are highly anisotropic with a high AO figure of merit thanks to a high photoelastic constant and slow acoustic velocity. Their wide spectral range of transparency are 0.35 – 20 µm, 0.4 – 30 µm and 0.45 – 40 µm respectively. Some prototype devices have been fabricated with single crystal of these materials recently grown[27-28].

2. AOTF CRYSTAL CONSIDERATION

AOTF crystal is an electronically controlled agile device that filters incident white light into narrow spectral band of light at a specific wavelength determined by RF signal. Wavelength of the filtered spectral band can be tuned without any physical movement of the filter by changing the frequency of the applied RF signal, making it a no-moving-parts robust and fast tunable filter. Principles of that filter operation are based on the well-known phenomenon of anisotropic diffraction of light by acoustic wave propagation in a birefringent crystal[29-32]. As shown in the figure 1, an AOTF crystal is fabricated by bonding a piezoelectric transducer to a specially cut birefringent high quality single crystal. When an RF signal is applied to the transducer, it produces an ultrasonic wave that travels through the crystal with acoustic frequency equal to the RF signal. This establishes a diffraction grating in the crystal with a velocity specific to the material and a grating period equal to the acoustic wave's period. An acoustic absorber absorbs the sound wave after its transmission into the crystal. The spectral bandwidth of the diffracted light depends upon diffracted wavelength, birefringence of the material, length of the transducer, acoustic cut angle and geometry of the wide-angle AO diffraction.

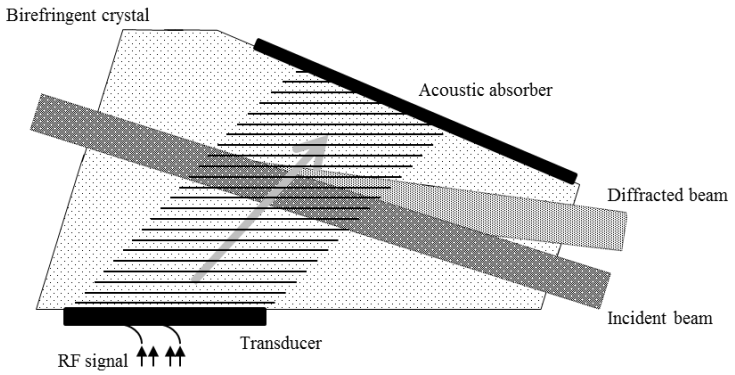

Figure 1 AOTF crystal operation principles based on a phenomenon of anisotropic diffraction of light by acoustic wave propagation in a birefringent crystal

So far, TeO_2 is the best AO material to design imaging filters due to its large M_2 value equal to 1200×10^{-18} s^3/g and its difference between the extraordinary and ordinary refractive indices relatively high. For TeO2, $n_o = 2.26$ and $n_e = 2.41$, giving a birefringence $\Delta n = 0.15$. Due to its large M_2 value, filters designed in TeO2 operate with high efficiency at relatively low applied power. Unfortunately, it cannot be used for AOTF devices operating above 5 µm. The three mercurous halide crystals[33] have a tetragonal crystalline structure class with the point group D(4*h*) and the space group 4/*mmm*. The mercurous halides have the same uniaxial crystal structure as TeO_2 and design considerations can draw upon the TeO_2 AOTF designs which have been discussed extensively in the literature[10-15].

As seen in Table 1, those materials have really high birefringence and have anomalously slow shear wave acoustic velocities of propagation along the [110] plane[24]. The lowest velocities are obtained for shear propagation along the [110] plane and are respectively : 347 m/s for Hg_2C1_2, 273 m/s for Hg_2Br_2, and 254 m/s for Hg_2I_2. The previously lowest recorded velocities (under normal conditions) were 616 m/s for $Te0_2$, 520 m/s for $T1_3PSe_4$ and 600 m/s for $T1_3AsS_4$. Shear velocity is significantly anisotropic, which leads to a very large walk-off angle between acoustic wave propagation and energy flow. Birefringence of those materials is high with 0.66 for Hg_2Cl_2, 0.86 for Hg_2Br_2 and 1.48 for Hg_2I_2. Those materials are optically positive uniaxial crystals, i.e. n_e is larger than n_o. Large birefringence and slow velocity properties are attributed to the strong anisotropy of the lattice field and the nature of the heavy Hg^{2+} ion. In this structure, parallel chains of linear X-Hg-Hg-X molecules are aligned along the direction of the crystallographic C axis. Bond between adjacent molecules is a Van der Waals type, while intramolecular bonding is mainly covalent. This

structural configuration generates strong photoelastic, elastic, and optical anisotropies in those crystals. Moreover, components of the photoelastic tensor of the calomel[1] are also quite large, p_{11} = 0.551, p_{12} = 0.44, and p_{31}= 0.137, as compared to p_{11} = -0.0074, p_{12} = 0.187 and p_{31} = 0.0905 in TeO2. Although various research works had measured and computed mercurous halide crystals main parameters[34-40], one component stay even nowadays unknown, the p_{44} component of the photoelastic tensor. Even by using well-known design methods of TeO_2 AO cells, this missing component value doesn't allow converge numerical computations toward a single optimum solution of diffraction efficiency. Therefore, it is reasonable to conclude that mercurous chloride may be considered as a promising material for a variety of applications in AO devices.

Material	Transparency window (µm)	Refractive indices	Acoustic velocity (x10^5 cm/s)	Density (g/cm^3)	Figure of merit (x10-18 s^3/g)
TeO_2	0.35 – 4.5	n_o=2.26 ; n_e=2.41	0.62	6.0	1200
Hg_2Cl_2	0.35 – 20	n_o=1.96 ; n_e=2.62	0.35	7.18	1050
Hg_2Br_2	0.40 – 30	n_o=2.21 ; n_e=2.98	0.27	7.31	3900
Hg_2I_2	0.45 – 40	n_o=2.43 ; n_e=3.91	0.25	7.70	4800

Table 1 table of key parameters of mercurous halide crystals compared to tellurium dioxide.

From Table 1 it is clear that mercurous halide crystals have a large transparency region and really high figure of merit. We could fabricate AOTFs operating from the visible to the LWIR using anyone of these halides as Hg_2Cl_2 by suitably bonding multiple transducers to cover a large spectral region. Although Hg_2I_2 and Hg_2Br_2 crystals have really high qualities for AO devices, some development research works are still ongoing to be able to grow longer robust crystals[26, 41]. At the present time research is ongoing in finding the most suitable bonding media with mercury based crystals which will be stable over a long time[42, 43].

3. NUMERICAL MODEL AND RESULTS

3.1 Refractive indexes

Dispersion formulas of refractive indexes can be written in function of the wavelength filtered. For the calomel crystal, this change of refractive indexes has been reported by a European consortium of MINERVA project[44] using a polynomial fitting from experimental data:

$$n_o = 1.898 + 1.5 \times 10^{-2} E_{ph}^2 + 3.7 \times 10^{-4} E_{ph}^4 + 7 \times 10^{-6} E_{ph}^6 + 4 \times 10^{-7} E_{ph}^8 + 5 \times 10^{-8} E_{ph}^{10} \quad (1)$$

$$n_e = 2.444 + 3.87 \times 10^{-2} E_{ph}^2 + 1.73 \times 10^{-3} E_{ph}^4 + 4.5 \times 10^{-5} E_{ph}^6 + 3.46 \times 10^{-6} E_{ph}^8 + 3 \times 10^{-7} E_{ph}^{10} \quad (2)$$

With the photon energy E_{ph}[eV] defined by:

$$E_{ph} = \frac{hc}{\lambda} \quad (3)$$

Where h is the Planck's constant, c is the speed of light and λ is the filtered wavelength in the vacuum.

3.2 Acoustic Velocity along tZ plane

The t[110]-Z[001] plane is the preferred plane for the slow shear AO interaction[45] and it is selected by rotating the references plan about the Z axis of π/4 from [100] direction. The rotation of the reference axis is applied to obtain the new elastic stiffness constant matrix for this rotation:

$$[c'_{kl}] = \begin{bmatrix} c'_{11} & c'_{12} & c_{13} & 0 & 0 & 0 \\ c'_{12} & c'_{11} & c_{13} & 0 & 0 & 0 \\ c_{13} & c_{13} & c_{33} & 0 & 0 & 0 \\ 0 & 0 & 0 & c_{44} & 0 & 0 \\ 0 & 0 & 0 & 0 & c_{44} & 0 \\ 0 & 0 & 0 & 0 & 0 & c'_{66} \end{bmatrix} \quad (4)$$

Where:

$$c'_{11} = \frac{c_{11}+c_{12}+2c_{66}}{2} \quad (5)$$

$$c'_{12} = \frac{c_{11}+c_{12}-2c_{66}}{2} \quad (6)$$

$$c'_{66} = \frac{c_{11}-c_{12}}{2} \quad (7)$$

The velocity of acoustic wave for a given direction of θ_a , which is defined from [110] direction, for the slow shear mode can be defined as :

$$V_S^2 = V_t \cos^2(\theta_a) + V_Z \sin^2(\theta_a) = \frac{c'_{66}\cos^2(\theta_a)+c_{44}\sin^2(\theta_a)}{\rho} \quad (8)$$

The Acousto-optic interaction plane considered is the t-Z plane. In the literature, the elastic stiffness constant values[28] are c_{11} = 1.8925 x10^{10} N/m², c_{12} = 1.7192 x10^{10} N/m², c_{13} = 1.563 x10^{10} N/m², c_{33} = 8.037 x10^{10} N/m², c_{44} = 0.8456 x10^{10} N/m² and c_{66} = 1.225 x10^{10} N/m². Velocities of the slow shear acoustic waves in each direction are equal to V_t = 384 m/s and V_Z = 1084 m/s, respectively.

3.3 Phase matching condition

Efficient Acousto-optic interaction is obtained when the phase matching condition between acoustic waves and incident electromagnetic radiation is satisfied and described by equations:

$$K_d(\lambda, f, \theta_a) = K_a(f, \theta_a) + K_i(\lambda, \theta_a) \quad (9)$$

Where:

$$K_{d,i} = \frac{2\pi n_{d,i}}{\lambda} \quad (10)$$

$$K_a = \frac{2\pi V(\theta_a)}{f} \quad (11)$$

With $n_{d,i}$ the refractive indexes of incident and deflected beams, $V(\theta_a)$ the acoustic velocity and f the RF applied to the ultrasonic transducer. The phase matching condition described above is graphically represented in the K-space diagram below, where k_i is the incident light, k_d is the first diffracted order, k_a is the acoustic wave momenta.

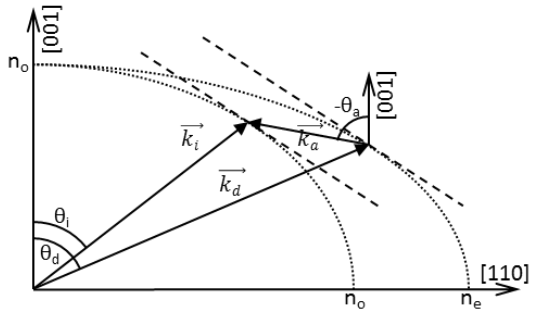

Figure 2 K-space diagram of an AO interaction respecting the phase matching condition between incident and diffracted electromagnetic waves and acoustic wave.

From Eq.9, it is possible to define the tuning relation, which is the relation between RF frequency applied to the transducer and the wavelength of the diffracted order for broadband incident light. This relation is defined by:

$$\boldsymbol{\lambda = \frac{V(\theta_a)}{f}\sqrt{n_i^2(\lambda) + n_d^2(\lambda) - 2n_i(\lambda)n_i(\lambda)\cos(\theta_d - \theta_i)}} \tag{12}$$

An infinite number of configurations of the AO interaction exist, but in practice some constraints are applied in order to optimize one of the parameters in real devices such as: resolution, field of view, RF drive power versus diffraction efficiency, etc. The parallel tangent matching condition[29] is defined as:

$$\tan(\theta_d) = \left(\frac{n_d}{n_i}\right)^2 \tan(\theta_i) \tag{13}$$

Where tangents refractive index surfaces are parallel for the incoming and diffracted light, thus a constraint is set between θ_i and θ_d. It's possible to determine input direction for an arbitrary propagation of the phase velocity of the acoustic wave. Phase matching condition is derived from a given θ_a and the input angle of electromagnetic radiation:

$$\tan(\theta_a) = \frac{\left(\frac{n_e}{n_o}\right)^2 \tan(\theta_i) - \sin(\theta_i)\sqrt{1+\left(\frac{n_e}{n_o}\right)^2 \tan^2(\theta_i)}}{1-\cos(\theta_i)\sqrt{1+\left(\frac{n_e}{n_o}\right)^2 \tan^2(\theta_i)}} \tag{14}$$

From the solution of the above equations, it's possible to determine θ_i and consequently θ_d. The phase matching condition could also be solved by defining θ_i to determine the range of θ_a where the parallel tangent matching condition is satisfied for a given wavelength.

3.4 AO interaction's efficiency

Diffraction efficiency of the AO interaction is proportional to the RF power applied to the ultrasonic transducer, when the phase matching condition is satisfied, and theoretically it can be estimated[45] by :

$$\eta = \sin^2 \frac{\pi}{\lambda}\sqrt{\frac{M_2\, L\, P}{2\, H}} \tag{15}$$

Where L/H is the dimensional ratio of the transducer, P is the RF Power, λ is the wavelength of diffracted order and M_2 is the Acousto-optic figure of merit defined as:

$$M_2 = \frac{n_i^3 n_d^3 p_{eff}^2}{\rho V^3(\theta_a)} \tag{16}$$

With p_{eff} the effective photoelastic constant, $V(\theta_a)$ the phase velocity of acoustic wave, ρ the density and $n_{i,d}$ the refractive indexes of incident and diffracted beams respectively. Effective photoelastic constant is obtained from tonsorial equation; therefore it is related to the geometry of the AO interaction. Calomel photoelastic constant matrix[46-47] is determined by the tetragonal crystal structure as:

$$[P_{ij}] = \begin{bmatrix} p_{11} & p_{12} & p_{13} & 0 & 0 & 0 \\ p_{12} & p_{11} & p_{13} & 0 & 0 & 0 \\ p_{13} & p_{13} & p_{33} & 0 & 0 & 0 \\ 0 & 0 & 0 & p_{44} & 0 & 0 \\ 0 & 0 & 0 & 0 & p_{44} & 0 \\ 0 & 0 & 0 & 0 & 0 & p_{66} \end{bmatrix} \tag{17}$$

In the literature[28], the photoelastic constant values are $p_{11} = 0.551$, $p_{12} = 0.44$, $p_{13} = 0.137$, $p_{33} = 0.01$, p_{44} = unknown and $p_{66} = 0.047$. Effective photoelastic constant in the case of an interaction occurring in the plane tZ can be estimated by equation:

$$p_{eff} = p_{44}\cos(\theta_a)\sin(\theta_d) - \frac{p_{11}-p_{22}}{2}\sin(\theta_a)\cos(\theta_d) \tag{18}$$

This general expression of p_{eff} for tetragonal crystals is used to estimate the Acousto-optic figure of merit for a given AO interaction.

3.5 Model principles and results

AO interaction model objectives are in a first hand to be able to make an evaluation of configurations that allow highest value of diffraction efficiency. In a second hand, to be able to make the criticality control points of the change of several main parameters. Those optima configurations are found for a certain crystal material. Calomel crystal (Hg_2Cl_2) has a serious flaw, its photo-elastic tensor is not complete and the p_{44} component is unknown from the literature. Our model takes account of this flaw. Overview schema below presents main nodes of calculation with main decisions criteria to eliminate unsatisfactory configurations. From the material's parameters, it evaluate diffraction efficiency for each AO configuration (θ_i, θ_d, θ_a, L/H, P_{RF}, f_{RF}), sweeping the p_{44} value. Thus is made for an electromagnetic wave with a wavelength from 0.4 to 20 µm. To achieve this computation, the model sweeps value of incident angle of broadband light, validate for each the RF frequency range to access all wavelengths. Then it starts the diffraction efficiency calculation in function of interaction dimension ratio between the two waves and the acoustic power used. That research tries to point out impact of several parameters of AO configuration design on diffraction efficiency. In particular, understand the impact of the unknown value of p_{44}, the impact of the acoustic power signal used and the interaction size ratio between the two waves.

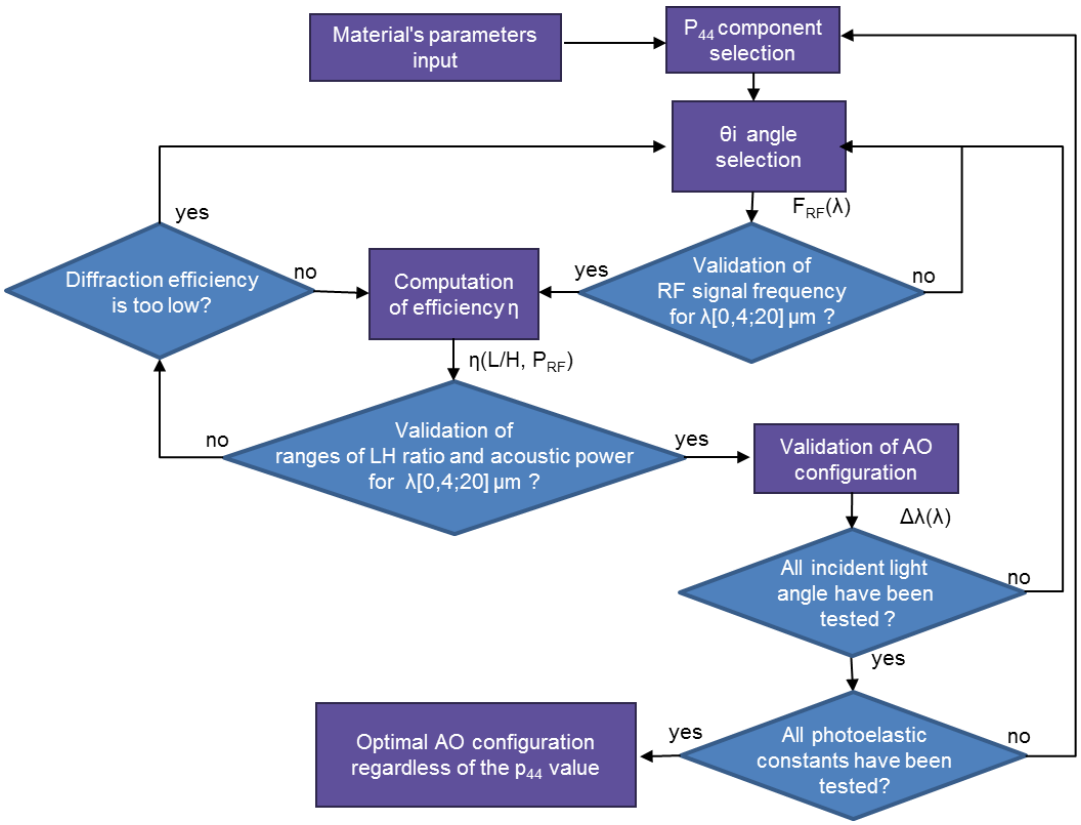

Figure 3 principle schema of numerical model, in square shapes the calculation nodes and in diamond shapes the feedback loops.

In figure 4, we first compare the AO diffraction efficiency in function of output diffracted wavelength sweeping the p_{44} value from -0.5 to 0.5. Repeating those measurements for several incident light angle values shows that we start to be really affected by the unknown p_{44} value with incident angle of broadband light superior to 5 degrees with a $\Delta\eta \sim 10\%$ for wavelength superior at 12 µm. This sensitivity to p_{44} value increases drastically with the incident angle. And $\Delta\eta$ reach 50% when $\theta_i = 10°$ and 100% when $\theta_i = 20°$. With those results, we clearly see that the unknown value of p_{44} have a serious impact on broadband performance of AOTF crystal of calomel when the incident angle is high.

For next studies, we apply the atmospheric transmission in the model to be able to see and evaluate impact that would have the interaction size ratio and acoustic power on the atmospheric windows. The atmospheric transmission factor dataset was used from the planetary spectrum generator of NASA website[48].

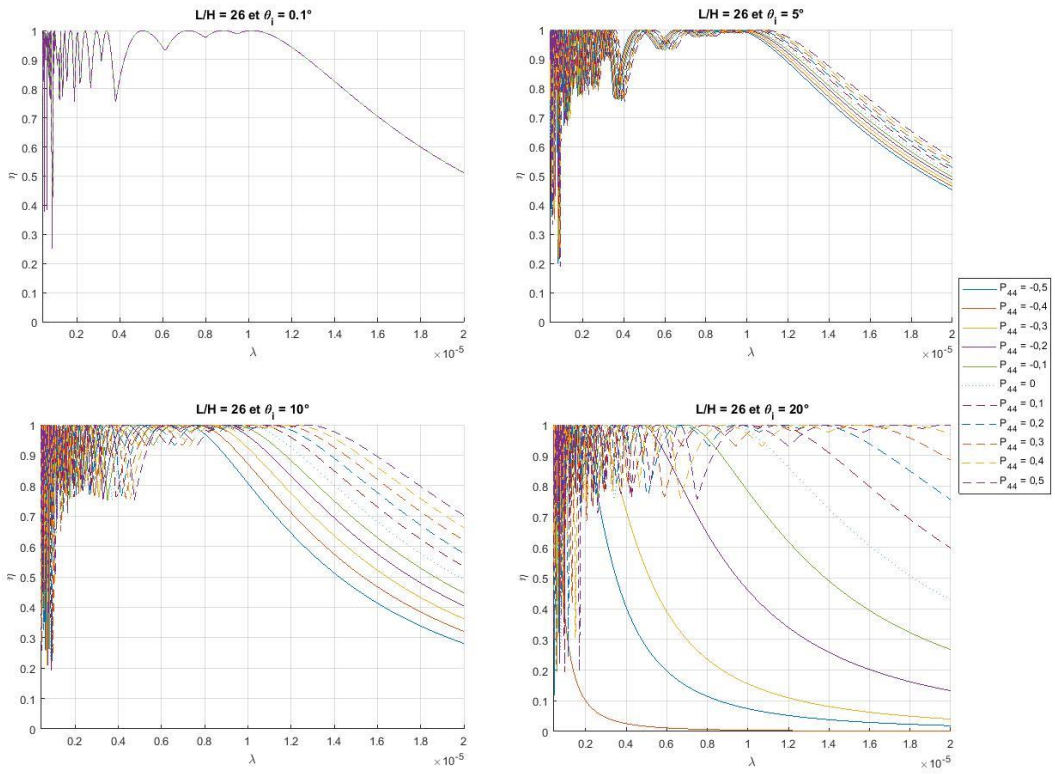

Figure 4 Impact of p_{44} value on diffraction efficiency for several angles of incident broadband light.

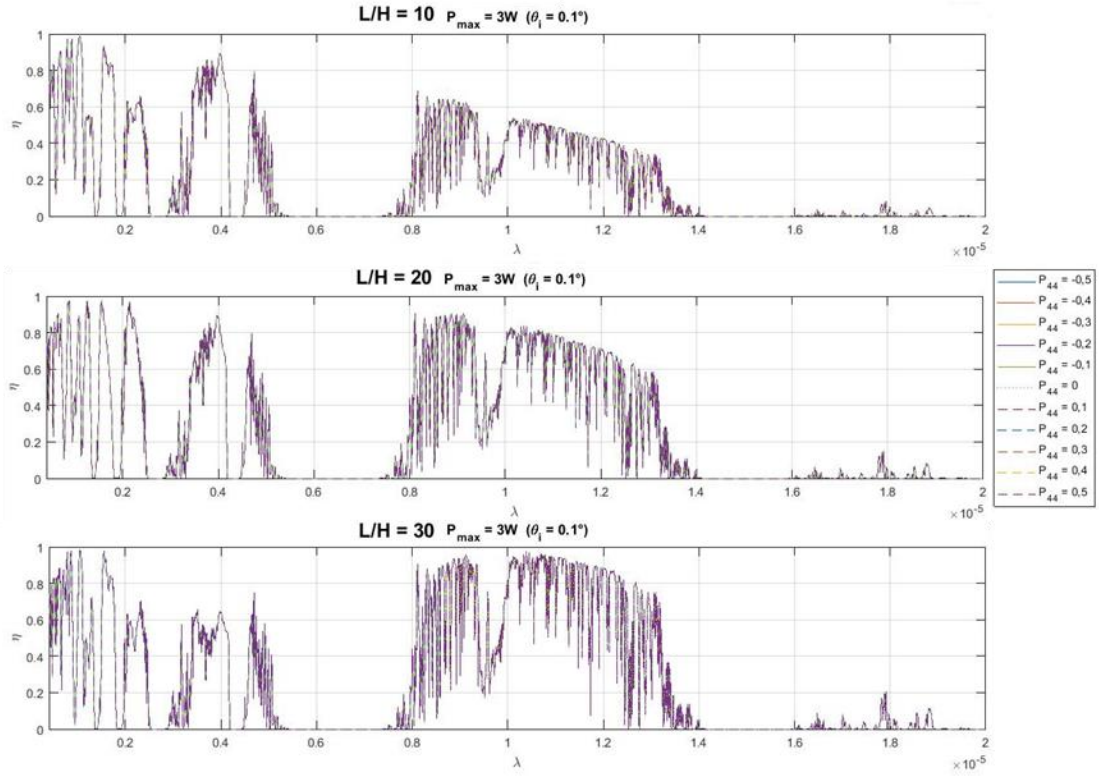

Figure 5 Impact of size interaction ratio on AO diffraction efficiency

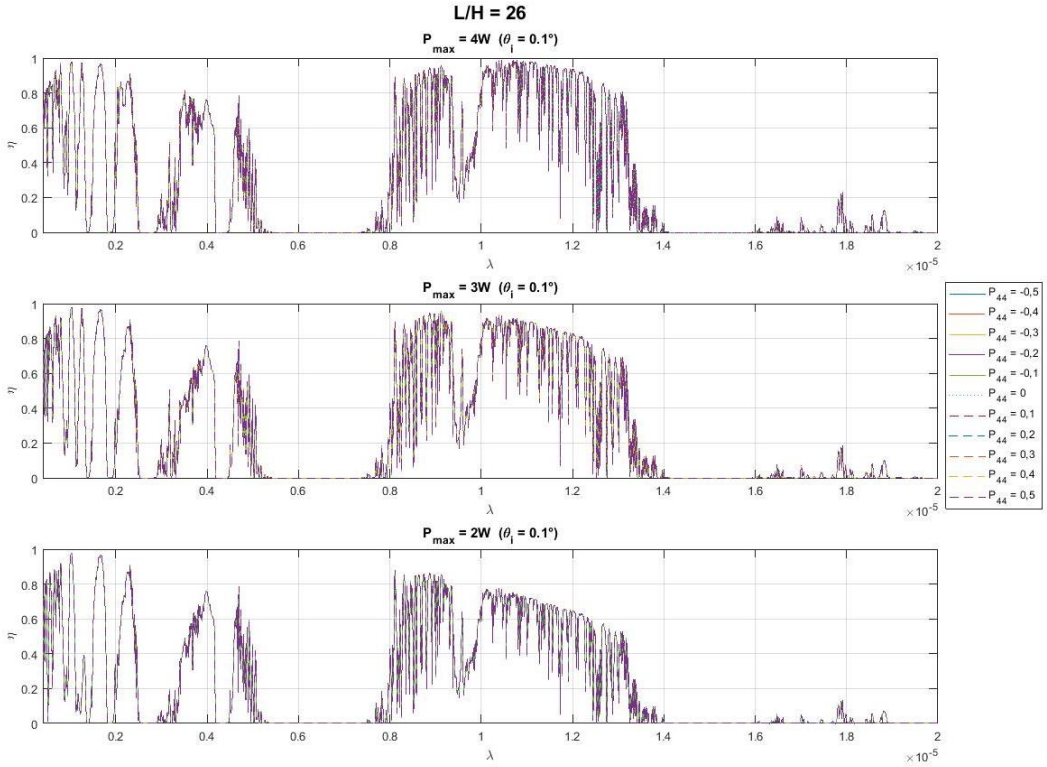

Figure 6 Impact of acoustic power on AO diffraction efficiency

In figure 5, we compare the AO diffraction efficiency in function of output diffracted wavelength for several interaction size ratio values. From the equations, increase of L/H ratio will be reciprocal to an increase of diffraction efficiency. This is true for high values of wavelength beyond 5 µm. Unfortunately, increase of the size ratio will also cause a translation movement in the diffraction efficiency peaks that are important in low wavelength below 5µm. In particular, the important decrease of diffraction efficiency visible in Figure 4 at 3.8 µm that will move from 3 to 4 µm for a respective variation of L/H from 10 to 30. We see this impact in this region on the transmission windows that decrease instead of increase with L/H value.

Represented in figure 6, we compare the AO diffraction efficiency in function of output diffracted wavelength for several acoustic powers. As expected, increase of Acoustic power will also increase the AO diffraction efficiency for every wavelength, the previous effect of peaks shifting doesn't occur with this parameter.

4. DISCUSION

An AOTF is a device with no-moving parts that can provide an electronically tuned bandpass filter by the application of a RF signal. AOTF are used in the development of hyperspectral imagers from the UV to the LWIR. In the LWIR there is a global investigation on efficient solutions for AOTF. Crystals of mercurous halides are candidates that demonstrate an advantage in this spectral domain, thanks to a broadband transparency and a fairly large value of their figure of merit. In our works, we develop a numerical tool to compute the diffraction efficiency of AO configurations in those crystals, in particular in the calomel crystal (Hg_2Cl_2). Mercurous halide crystals have the flaw that their photoelastic tensor are not complete, the component p_{44} is unknown from the literature. Our research reports that diffraction efficiency is less sensitive to this p_{44} value in a AO configuration with low value of incident light angle. We also report that the choice of increasing interaction size ratio doesn't mean a constant increase of diffraction efficiency in certain wavelengths. In particular in the region below 5µm where a shift of diffraction efficiency peaks exist. Industrial development of those crystals has recently started and presents an excellent opportunity to prospect feasibility of such AOTF. Depending of the use case for AOTF crystals and the spectral region of interest, it will be a compromise between acoustic power and dimension size ratio increase to find an optimal AO configuration.

REFERENCES

[1] I. C. Chang, "Tunable acousto-optic filters: an overview," Proc. SPIE 90, 12-22, 1976.
[2] J. Xu and R. Stroud, Acousto-Optic Devices (Wiley, New York, N.Y., 1992).
[3] A. Goutzoulis and D. Pape, Designing and Fabrication of Acousto-Optic Devices (Marcel Dekker, New York, N.Y., 1994).
[4] N. J. Berg and J. M. Pellegrino, Acousto-Optic Signal Processing: Theory and Implementation (Marcel Dekker, New York, N.Y., 1996).
[5] V. Voloshinov, A. Tchernyatin, E. Blomme and 0. Leroy, "A dozen of Bragg effects in tellurium dioxide single crystal," Proc. SPIE 3581, 141–152, 1998.
[6] N. Gupta, and V. Voloshinov, "Deep UV spectral imaging characterization of an improved KDP acousto-optic tunable filter," J. Opt. 16, 035301, 2014.
[7] V. B. Voloshinov and N. Gupta, "Ultraviolet/Visible Imaging Acousto-Optic Tunable Filters in KDP," Appl. Opt. 43, 3901–3909, 2004.
[8] V. B. Voloshinov and N. Gupta, "Investigation of magnesium fluoride crystals for imaging acousto-optic tunable filter applications," Appl. Opt. 45, 3127–3135, 2006.
[9] N. Gupta, "Acousto-optic tunable filters for Infrared Imaging," Proc SPIE 5953, 59530O 1–10, 2005.
[10] N. Gupta, R. Dahmani, and S. Choy, "Acousto-optic tunable filter based visible-to-near-infrared spectropolarimetric imager," Opt. Eng. 41, 1033–1038, 2002.
[11] N. Gupta and D. R. Suhre, "AOTF imaging spectrometer with full Stokes polarimetric capability," Appl. Opt. 46, 2632–2037, 2007.
[12] V. B. Voloshinov and N. Gupta, "Acousto-optic imaging in the mid-infrared region of the spectrum," Proc. SPIE 3900, 62–73, 1999.
[13] N. Gupta and V. B. Voloshinov, "Development and Characterization of Two-Transducer Imaging Acousto-Optic Tunable Filters with Extended Tuning Range," Appl. Opt. 46, 1081-1088, 2007.
[14] Javier Calpe-Maravilla, Javier Calpe-Maravilla, Joan Vila-Frances, et al. "400- to 1000-nm imaging spectrometer based on acousto-optic tunable filters", Proc. SPIE 5570, Sensors, Systems, and Next-Generation Satellites VIII, (4 November 2004)
[15] Rula Tawalbeh; David G. Voelz; David A. Glenar; et al. "Infrared acousto-optic tunable filter point spectrometer for detection of organics on mineral surfaces" Optical Engineering, 52(6), 063604 (2013)
[16] D. R. Suhre, N. Gupta and M. Gottlieb, "LWIR spectral imager with an 8-cm-1 passband acousto-optic tunable filter," Optical Engineering, 44(9), 094601 (2005).
[17] N. B. Singh, D. Suhre, N. Gupta, W. Rosch, and M. Gottlieb, "Performance of TAS crystal for AOTF Imaging," Jour. Crystal Growth 225, 124–128, 2001.
[18] J. D. Feichtner, M. Gottlieb, and J. J. Conroy, "Tl3AsSe3 noncollinear acousto-optic filter operation at 10 μm," Appl. Phys.Lett. 34, 1–3 (1979).
[19] D. Suhre and E. Villa, "Imaging spectroradiometer for the 8–12 μm region with 3cm−1 passband acousto-optic tunable filter," Appl. Opt. 37(12), 2340–2345 (1998).
[20] N. B. Singh, D. Kahler, D. J. Knuteson, M. Gottlieb, D. Suhre, A. Berghmans, B. Wagner, J. Hedrick, T. Karr, and J. J. Hawkins, "Operational characteristics of a longwavelength IR multispectral imager based on an acousto-optic tunable filter," Opt. Eng. 47, 013201 (2008).
[21] M. Silvestrova, C. Barta, G. F. Dobrzhanskii, L. M. Belyaev, and Y. V. Pisarevskii, "Acousto-optical properties of calomel crystals Hg2C12," Soy. Phys. Crystallogr. 20, 1062—1069 (1975).
[22] N. B. Singh, R. H. Hopkins, R. Mazeisky, M. Gottlieb, and E. Metz, 'Growth of large mercurous chloride single crystals by sublimation," J. Cryst. Growth 74, 667—669 (1986).
[23] M. Gottlieb, A. P. Goutzoulis, and N. B. Singh, "Mercurous chloride (Hg2Cl2) acousto-optic devices," Proc. IEEE Ultrasonics. Sym., 423—427 (1986).Davis,
[24] M. Gottlieb, A. Goutzoulis, and N. Singh, "High-performance acousto-optic materials: Hg2Cl2 and PbBr2," Opt. Eng. 31, 2110–2117 (1992).
[25] N. B. Singh and R. Mazelsky, "Development of mercurous halides for acousto-optic devices," Curr. Top. Cryst. Growth Res.2, 435–444 (1995).
[26] J. Kim, S. B. Trivedi, J. Soos, N. Gupta, andW. Palosz, "Development of mercurous halide crystals for acousto-optic devices," Proc. SPIE 6661 66610B (2007).

[27] D. J. Knuteson, N. B. Singh, M. Gottlieb, D. Suhre and N. Gupta, "Crystal Growth, Fabrication and Design of Mercurous Bromide Acousto-Optic Tunable Filters" Opt. Eng. .46(6), 064001-064006, 2007.
[28] J. Kim, S. Trivedi, B., J. Soos, W. Palosz, and N. Gupta, "Development of Mercurous Halide Crystals for Acousto-Optic Devices," Proc. SPIE 6661, 66610B 1–12, 2007.
[29] Chang, I. C., "Tunable acousto-optic filters: an overview," Proc. SPIE 90, 12–22 (1977).
[30] Xu, J. and Stroud, R., [Acousto-Optic Devices], Wiley, New York (1992).
[31] Goutzoulis, A. and Pape, D., [Design and Fabrication of Acousto-Optic Devices], Marcel Dekker Inc., New York, NY (1994).
[32] Gupta, N., "Chapter 32 : Acousto-Optics", in [Optical Engineer's Desk Reference], ed. W. Wolfe, Optical Society of America, Washington D.C. (2003).
[33] A. P. Goutzoulis and M. Gottlieb, "Characteristics and design of mercurous halide Bragg cells for optical signal processing,' ' Opt. Eng. 27(2), 157—163 (1988).
[34] C. Barta, "Preparation of mercurous chloride monocrystals,' ' Krist. Tech. 5, 541—549 (1970).
[35] I. M. Sylvestrova, C. Barta, G. F. Dobrzhansbii, L. M. Belyaev, and Y. V. Pisarevskii, "Elastic properties of Hg2C12 crystals,' ' Soy. Phys.Crystallogr. 20, 221—224 (1975).
[36] I. M. Silvestrova, C. Barta, G. F. Dobrzhansbii, L. M. Belyaev, and Y. V. Pisarevskii, ' 'Acousto-optical properties of calomel crystals Hg2Cl2," Soy. Ploys. Crystallogr. 20, 649—65 1 (1975).
[37] G. Barta and J. Trnka, ' 'New types of polarizers made from crystals of the calomel group," Cryst. Res. Technol. 17, 431—438 (1982).
[38] M. Gottlieb, A. P. Goutzoulis, and N. B. Singh, "Fabrication and characterization of mercurous chloride acousto-optic devices,' ' Appl.Opt. 26, 4681—4687 (1987).
[39] C. Barta and C. Barta, Jr. , ' 'Physical properties of single crystals of the calomel group,' ' in Growth and Characterization of Acousto-Optical Materials, Materials Science Forum, Vol. 61, N. B. Singh, Ed. , Trans Tech Publications, Zurich (1990).
[40] G. B. Brandt, N. B. Singh, and M. Gottlieb, "Mercurous halides for long time delay Bragg cells," Proc. SPIE 1454, 336—343 (1991).
[41] J. Kim, S. B. Trivedi, J. Soos, N. Gupta, andW. Palosz, "Growth of Hg2Cl2 and Hg2Br2 single crystals by physical vapor transport,"J. Cryst. Growth 310, 2457–2463 (2008).
[42] Valle, Stefano (2017) Design and application of high performance Acousto-Optic Tunable Filters. EngD thesis, University of Glasgow.
[43] Neelam Gupta, "Materials for imaging acousto-optic tunable filters" Proc. SPIE 9100, Image Sensing Technologies: Materials, Devices, Systems, and Applications, 91000C (21 May 2014)
[44] http://minerva-project.eu/
[45] Xu J, Stroud R. Acousto-optic devices: principles, design, and applications. Wiley series in pure and applied optics. Wiley; 1992.
[46] J. Xu and R. Stroud, Acousto-Optic Devices (Wiley, 1992).
[47] J. F. Nye, Physical Properties of Crystals (Masson, 1974).
[48] https://psg.gsfc.nasa.gov/